inorganics

MDPI

Article

Synthesis and Structural Characterization of $Ba_7Li_{11}Bi_{10}$ and $AE_4(Li,Tr)_7Pn_6$ (AE = Sr, Ba, Eu; Tr = Ga, In; Pn = Sb, Bi)

Dickson O. Ojwang and Svilen Bobev *

Department of Chemistry and Biochemistry, University of Delaware, Newark, DE 19716, USA; dojwa@udel.edu
* Correspondence: bobev@udel.edu; Tel.: +1-302-831-8720

Received: 12 September 2018; Accepted: 28 September 2018; Published: 6 October 2018

Abstract: Reported are the synthesis and crystal structure of $Ba_7Li_{11}Bi_{10}$, a new ternary compound crystallizing in its own type with the monoclinic space group $C2/m$ (a = 18.407(3) Å, b = 5.0258(9) Å, and c = 18.353(3) Å; β = 104.43(1)°; Pearson symbol $mS56$), and those of the structurally related quaternary phases $Ba_4(Li_{1-x}Ga_x)_7Sb_6$, $Ba_4(Li_{1-x}In_x)_7Sb_6$, $Ba_4(Li_{1-x}In_x)_7Bi_6$, and $Eu_4(Li_{1-x}In_x)_7Bi_6$ (crystallizing in the $Eu_4Li_7Bi_6$ structure type with the same monoclinic space group $C2/m$ (a = 18.4045(13)–17.642(4) Å, b = 5.012(4)–4.8297(10) Å, and c = 13.2792(10)–12.850(3) Å, β = 126.80(1)–125.85(1)°; Pearson symbol $mS34$). All studied compounds are identified among the products of the high-temperature reactions of the corresponding elements. Both types of crystal structures are based on corner- and edge-linked Li-centered Sb_4 (or Bi_4) tetrahedra, Sb_6 (or Bi_6) octahedra, and Sb_2 or Bi_2 dumbbells. Given the similarities between the two structures, it might be proposed that they represent the simplest members of a potentially large homologous series described with the general formulae $(BaLi_3Sb_2)_n(Ba_3Li_4Sb_4)_m$ or $(BaLi_3Bi_2)_n(Ba_3Li_4Bi_4)_m$, where the more complicated "7-11-10" phase is the member with n = 2 and m = 1, while the "4-7-6" one is the intergrowth of the two components in an equal ratio. The computed electronic band structures of $Ba_7Li_{11}Bi_{10}$ and idealized $Ba_4Li_7Bi_6$ (a model for $Ba_4(Li_{1-x}In_x)_7Bi_6$) are also discussed.

Keywords: antimonides; bismuthides; crystal structure; Zintl phases

1. Introduction

Zintl phases represent a diverse class of compounds with complicated crystal and electronic structures. They display a wide variety of traits and they are potentially promising candidates for electronic, magnetic, superconductive, semiconductive, and thermoelectric materials, and therefore they have attracted much attention over the years [1–3]. To such, a host of Zintl compounds, e.g., $Eu_5In_2Sb_6$, $Ca_5Ga_2As_6$, Sr_3AlSb_3, $Ca_5In_2Sb_6$, and $Ca_5Al_2Sb_6$ etc., have been explored as thermoelectric materials because of their low lattice thermal conductivities [4–8]. For over a decade, our group has been working on the synthesis, structural chemistry, and properties of Zintl phases and intermetallic compounds comprising alkali, alkaline-earth, or rare-earth metals, and the pnictogens (Pn), e.g., $Na_{11}Ca_2Al_3Sb_8$, $Ba_4Li_2Cd_3Pn_6$, $AE_3Al_2Pn_4$, and $AE_7Ga_2Sb_6$ (Pn = P, As, Sb; AE = Ca, Sr, Ba, Eu) [9–12]. Recent investigations of the $RELi_3Pn_2$, $AELiPn$, and $AE_3Li_4Pn_4$ (RE = rare-earth metals; AE = Ca, Sr, Ba, Yb; Pn = As, Sb, Bi) series led to the discovery of the unique monoclinic compound $Eu_4Li_7Bi_6$ (space group $C2/m$ with own structure type) [13]. Studying its structure, one might conclude that applying the Zintl–Klemm formalism to rationalize it; namely, the electron counting scheme $(Eu^{2+})_4(Li^+)_7([Bi_2]^{4-})(Bi^{3-})_4(h^+)$ (the symbol h^+ denotes an electron hole), leaves some open questions. First, what is the root cause for the apparent electron-deficiency in this case? Second, could that lack of charge-balance according to the Zintl–Klemm concept be an artifact of the over-simplified way that the

complex bonding is treated? In an earlier publication [13], we tried to address these issues by carrying out electronic structure calculations, which confirmed the perceived electron deficiency. In light of the very limited experimental data on this structure, it was proposed that $Eu_4Li_7Bi_6$ could be an example where Eu has a mixed oxidation state, or, it could be an impurity-stabilized phase.

This unexpected finding encouraged us to study analogous compounds by exploring the series $AE_4Li_7Pn_6$ (AE = Sr, Ba, Eu; Pn = Sb, Bi). The idea was that if Sr and Ba, alkaline-earth metals that have only one stable oxidation state, 2+, can form the same structure, the uncertainty surrounding the state of Eu would be lifted, and it would be established that the electron-deficiency is an inherent feature of the structure. At the same time, experiments aimed at making $AE_4(Li_{1-x}Ga_x)_7Pn_6$ and $AE_4(Li_{1-x}In_x)_7Pn_6$, isostructural to $AE_4Li_7Pn_6$ (but not isoelectronic) were carried out with the idea of verifying whether Li atoms can be partially substituted by small amounts of Ga or In, thereby tuning the number of valence electrons to the "proper" level. Ga and In were chosen because of the demonstrated tendency of these elements to mix in the crystal structures of related alkaline-earth metal lithium germanides and stannides, e.g., $AELi_{1-x}In_xGe_2$, $RE_4Li_{4-x}Sn_{4+x}$, and $Li_{9-x}EuSn_{6+x}$ [14–16].

Herein we describe the results of these studies, focusing on the crystal and electronic structures of the compounds $Ba_4(Li_{1-x}Ga_x)_7Sb_6$, $Ba_4(Li_{1-x}In_x)_7Sb_6$, $Ba_4(Li_{1-x}In_x)_7Bi_6$, and $Eu_4(Li_{1-x}In_x)_7Bi_6$, all of which show partial substitution of Li by Ga or In at a level of $x \approx 0.06$–0.08, i.e., near the electron-precise Zintl phase-like composition. In addition, the exploratory work in these systems allowed for the identification of a completely new ternary bismuthide, $Ba_7Li_{11}Bi_{10}$, which crystallizes with its own monoclinic structure type, $C2/m$. The electronic structure calculations of the idealized $Ba_4Li_7Bi_6$ (a model for the actual $Ba_4(Li_{1-x}In_x)_7Bi_6$) and $Ba_7Li_{11}Bi_{10}$ compounds are also presented.

2. Results and Discussion

2.1. Crystal Structure and Bonding in $Ba_4(Li_{1-x}Ga_x)_7Sb_6$, $Ba_4(Li_{1-x}In_x)_7Sb_6$, $Ba_4(Li_{1-x}In_x)_7Bi_6$, and $Eu_4(Li_{1-x}In_x)_7Bi_6$

All the compounds of the "4-7-6" variety crystallize in the monoclinic space group $C2/m$ with their own structure type [13]. There are a total of 34 atoms in the unit cell and two formula units, thus, the Pearson symbol of this structure is $mS34$.

A ternary compound with this structure was reported by us in 2014, namely $Eu_4Li_7Bi_6$ [13]. At that time, the structure was considered unique, although we noted the existence of the phase known as $Ba_8Li_{13}GaSb_{12}$, reported eight years earlier [17]. Because the latter was worked out in non-standard coordinate settings (the published Wyckoff sequence of the structure is $i8$ d) [17], ICSD references it as isotypic to the $Ce_4Mg_7Ge_6$-type structure [18]. Our analysis from 2014 of the bonding in $Eu_4Li_7Bi_6$ [13] and $Ce_4Mg_7Ge_6$ [18] indicated that although both have the same $C2/m$ space group and same number of atoms in the unit cell, the structures are sufficiently different and should not be considered isotypic. This conjecture is also supported by the standardized version of the coordinates, which shows that $Eu_4Li_7Bi_6$ and its herein presented analogs have an $i8$ c Wyckoff sequence. Furthermore, the refined structure of $Ba_4(Li_{1-x}Ga_x)_7Sb_6$ ($x \approx 0.08$, i.e., $Ba_4(Li_{0.92}Ga_{0.08})_7Sb_6$ = $Ba_4Li_{\sim 6.4}Ga_{\sim 0.6}Sb_6$) shows that the previously reported $Ba_8Li_{13}GaSb_{12}$ (=$Ba_4Li_{6.5}Ga_{0.5}Sb_6$) has the same structure as all other members of the "4-7-6" family of pnictides (Tables 1–3), and that the structures of the ternary rare-earth metal–magnesium germanides belonging to the $Ce_4Mg_7Ge_6$ structure type are related, but not identical.

Crystallographic data for several crystals from each of the $Ba_4(Li_{1-x}In_x)_7Sb_6$ and $Ba_4(Li_{1-x}In_x)_7Bi_6$ structures are listed in Table 2. The analogous information from two $Eu_4(Li_{1-x}In_x)_7Bi_6$ crystals is given in Table 3. In all cases, the refined parameters included the scaling factors, atomic coordinates, displacement parameters, and where applicable—the extinction coefficient and occupancy factors. Relevant interatomic distances in the $Ba_4(Li_{1-x}Ga_x)_7Sb_6$, $Ba_4(Li_{1-x}In_x)_7Sb_6$, $Ba_4(Li_{1-x}In_x)_7Bi_6$, and $Eu_4(Li_{1-x}In_x)_7Bi_6$ structures are displayed in Table 4. Points of specific interest will be discussed in detail later, here, but we just mention that all of the AE–Pn, Pn–Pn, and Li–Pn distances are distributed between 3.6487(6)–3.3394(6) Å, 3.0589(9)–2.8472(10) Å, and 3.4407(4)–2.799(9) Å, respectively. These

metrics are consistent with those reported for CaLiSb, BaLiSb, $Ba_3Li_4Sb_4$, SrLiBi, $Ba_3Li_4Bi_4$, and $Eu_4Li_7Bi_6$ [13,19–23].

Table 1. Selected crystal structure data and refinement parameters for $Ba_4(Li_{1-x}Ga_x)_7Sb_6$ [a].

Empirical Formula	$Ba_4Li_{6.65}Ga_{0.35(1)}Sb_6$
Formula weight, g·mol^{-1}	1356.69
Space group, Z	$C2/m$ (No.12), 2
λ, Å	0.71073
T, K	200(2)
a, Å	18.105(6)
b, Å	4.9319(15)
c, Å	13.023(4)
β, °	126.676(4)
V, Å^3	932.6(5)
ρ_{calc}, g·cm^{-3}	4.83
$\mu_{Mo\ K\alpha}$, cm^{-1}	174.5
Collected/independent reflections	5282/1162
R_{int}	0.0361
GOF on F^2	1.042
R_1 ($I > 2\sigma(I)$) [b]	0.0249
R_1 (all data) [b]	0.0285
wR_2 ($I > 2\sigma(I)$) [b]	0.0526
wR_2 (all data) [b]	0.0536
Largest peak/hole, e^- Å^{-3}	1.36/−1.37

[a] This is the same compound, previously reported as $Ba_8Li_{13}GaSb_{12}$, the structure of which was refined in non-standard coordinate settings [17], and as a result assigned erroneously in ICSD. Reported unit cell parameters for $Ba_8Li_{13}GaSb_{12}$: a = 18.065(1) Å, b = 4.9407(10) Å, c = 13.012(1) Å, β = 126.73(1)°, V = 930.8(2) Å^3. [b] $R_1 = \sum||F_o| - |F_c||/\sum|F_o|$; $wR_2 = [\sum[w(F_o^2 - F_c^2)^2]/\sum[w(F_o^2)^2]]^{1/2}$, where $w = 1/[\sigma^2F_o^2 + (0.0267P)^2]$, and $P = (F_o^2 + 2F_c^2)/3$. A CIF has been deposited with reference number CSD 1867165.

Table 2. Selected crystal structure data and refinement parameters for $Ba_4(Li_{1-x}In_x)_7Sb_6$ and $Ba_4(Li_{1-x}In_x)_7Bi_6$.

Empirical Formula	$Ba_4Li_{6.25}In_{0.75(1)}Sb_6$	$Ba_4Li_{6.45}In_{0.55(1)}Sb_6$	$Ba_4Li_{6.45}In_{0.55(1)}Sb_6$	$Ba_4Li_{6.55}In_{0.45(1)}Bi_6$	$Ba_4Li_{6.60}In_{0.40(1)}Bi_6$
Formula weight g·mol^{-1}	1409.35	1387.77	1387.43	1900.37	1894.97
Space group, Z			$C2/m$ (No.12), 2		
λ, Å			0.71073		
T, K			200(2)		
a, Å	18.172(5)	18.149(3)	18.146(3)	18.409(1)	18.440(3)
b, Å	4.9546(14)	4.9406(9)	4.9397(9)	5.0133(4)	5.0092(7)
c, Å	13.093(4)	13.082(2)	13.080(2)	13.282(1)	13.275(2)
β, °	126.799(3)	126.678(2)	126.680(2)	126.292(1)	126.271(2)
V, Å^3	944.0(5)	940.8(3)	940.3(3)	988.0(1)	986.3(2)
ρ_{calc}, g·cm^{-3}	4.96	4.90	4.90	6.39	6.38
$\mu_{Mo\ K\alpha}$, cm^{-1}	174.9	173.1	173.2	615.7	615.8
Collected/independent reflections	7140/1454	8997/1615	7141/1174	7507/1243	7524/1239
R_{int}	0.0296	0.0467	0.0399	0.0491	0.0821
GOF on F^2	1.066	1.060	1.037	1.039	1.064
R_1 ($I > 2\sigma(I)$) [a]	0.0187	0.0241	0.0220	0.0256	0.0368
R_1 (all data) [a]	0.0207	0.0289	0.0258	0.0278	0.0425
wR_2 ($I > 2\sigma(I)$) [a]	0.0410	0.0565	0.0491	0.0613	0.0904
wR_2 (all data) [a]	0.0420	0.0580	0.0504	0.0623	0.0936
Largest peak/hole, e^- Å^{-3}	2.17/−1.89	1.37/−1.36	1.20/−1.29	1.64/−1.48	2.75/−3.94

[a] $R_1 = \sum||F_o| - |F_c||/\sum|F_o|$; $wR_2 = [\sum[w(F_o^2 - F_c^2)^2]/\sum[w(F_o^2)^2]]^{1/2}$, where $w = 1/[\sigma^2F_o^2 + (AP)^2 + (BP)]$, and $P = (F_o^2 + 2F_c^2)/3$; A, B are the respective weight coefficients (see CIF in the supporting information). CIF have also been deposited with reference numbers CSD 1867166 and 1867167 (one from each composition).

Table 3. Selected crystal structure data and refinement parameters for $Eu_4(Li_{1-x}In_x)_7Bi_6$.

Empirical Formula	$Eu_4Li_{6.55}In_{0.45(1)}Bi_6$	$Eu_4Li_{6.60}In_{0.40(1)}Bi_6$
Formula weight, g·mol^{-1}	1958.85	1953.45
Space group, Z	$C2/m$ (No.12), 2	
λ, Å	0.71073	
T, K	200(2)	
a, Å	17.642(4)	17.607(3)
b, Å	4.8297(10)	4.8222(8)
c, Å	12.850(3)	12.826(2)
β, °	125.845(2)	125.929(2)
V, Å^3	887.6(3)	881.8(2)
ρ_{calc}, g·cm^{-3}	7.33	7.36
$\mu_{Mo\ K\alpha}$, cm^{-1}	736.7	740.9
Collected/independent reflections	8340/1491	6718/1113
R_{int}	0.0506	0.0468
GOF on F^2	1.053	1.119
R_1 ($I > 2\sigma(I)$) [a]	0.0278	0.0251
R_1 (all data) [a]	0.0332	0.0287
wR_2 ($I > 2\sigma(I)$) [a]	0.0576	0.0598
wR_2 (all data) [a]	0.0592	0.0609
Largest peak/hole, e^-Å^{-3}	2.21/−2.35	1.52/−2.34

[a] $R_1 = \sum||F_o| - |F_c|| / \sum|F_o|$; $wR_2 = [\sum[w(F_o^2 - F_c^2)^2] / \sum[w(F_o^2)^2]]^{1/2}$, where $w = 1/[\sigma^2F_o^2 + (AP)^2 + (BP)]$, and $P = (F_o^2 + 2F_c^2)/3$; A, B are the respective weight coefficients (see CIF in the supporting information). A CIF has been deposited with reference number CSD 1867168.

The overall structure is schematically shown in Figure 1. As seen in the structural representation, there are different coordination polyhedra. Li1, Li2, and Li3 atoms are all tetrahedrally coordinated by Sb, while Li4 is octahedrally coordinated. The polyhedra interact through edge and corner sharing. Naturally, because of the arrangement of these fused polyhedra, some relatively short Li–Li contacts arise (Li1–Li3 3.05(1) Å, Li1–Li4 2.98(3) Å). However, considering the Pauling single-bonded radius, r_{Li} = 1.225 Å [24], such distances are not indicative of strong bonding interactions. *Pn*1 atoms form $[Pn_2]^{4-}$ dimers (isoelectronic with the I_2 molecule), while *Pn*2 and *Pn*3 atoms exist as isolated Pn^{3-} ions. In the tetrahedra where Li is mixed and occupied with Ga or In, the distances to the closest neighbors vary from 2.867(5) to 3.071(2) Å. Note also that the Sb–Sb bond lengths are almost invariant of other structural parameters, which is indicative of strong covalent bonds; they vary in magnitude from 2.8427(13) to 2.8472(10) Å, and they are shorter than the 2.908 Å Sb–Sb distance found in elemental Sb [25]. The same can be said for the Bi–Bi bonding too, where the Bi–Bi distances are in the range 3.0443(8) to 3.0522(10) Å, which is shorter than the distances in elemental Bi [26]. However, this finding is not surprising, as similar values have been reported for KSb, $Ba_3Li_4Bi_4$, $Sr_3Li_4Sb_4$, $Eu_3Li_4Sb_4$, KBi, SrLiBi, $Ba_{21}Cd_4Bi_{18}$, and $Eu_4Li_7Bi_6$ [13,20,27–29]. The Ba atoms prefer sites with high coordination numbers, and they can be viewed as Ba^{2+} cations residing within channels of the $[Li_7Sb_6]$ and $[Li_7Bi_6]$ polyanionic sub-structure (exaggerating of course the covalency of the Li–Sb and Li–Bi bonds).

We also draw attention to the $Eu_4Li_{6.60}In_{0.40(1)}Bi_6$ structure and that of $Eu_4Li_7Bi_6$ as reported by our group in a previous study [13]. Rigorous assessment of the unit cell parameter and the interatomic distances show very clear differences, which attest to the structural response to the variation of the electron count (notice that the ionic radii of Li^+ and In^{3+} for the same coordination number 4 are very close, 0.59 and 0.62 Å, respectively [30], and geometric factors will not be expected to play a big role, especially at this level or with Li–In substitution). First, let us compare the unit cell parameters and volumes. They are the following: a = 17.558(3) Å, b = 4.8114(8) Å, c = 12.812(2) Å, β =126.035(2)°, V = 875.2(3) Å^3 for $Eu_4Li_7Bi_6$, and a = 17.607(3) Å, b = 4.8222(8) Å, c = 12.826(2) Å, β =125.929(2)°, V = 881.8(2) Å^3) for $Eu_4Li_{6.60}In_{0.40(1)}Bi_6$. The ca. 1% increase in the unit cell volume correlates well with some subtle changes in the bond distances and bond angles.

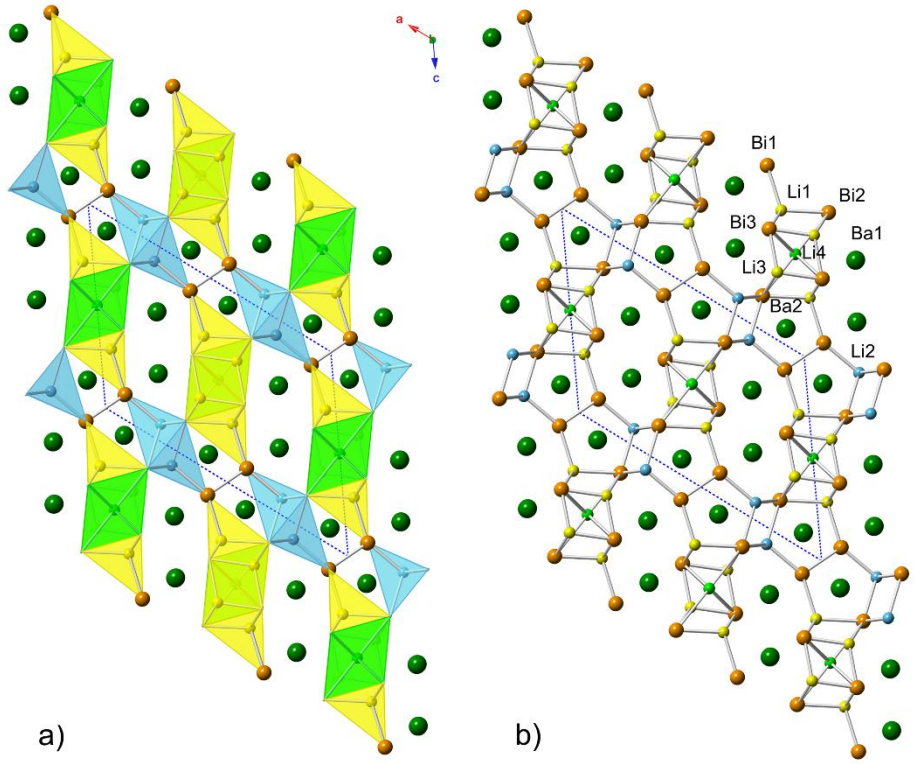

Figure 1. (**a**) Polyhedral representation of the crystal structure of the "4-7-6" family of pnictides, viewed down the crystallographic *b*-axis. The unit cell is outlined. The data used to represent the structure are taken from the refinement of $Ba_4Li_{6.55}In_{0.45(1)}Bi_6$. Different types of atoms are differentiated as follows: Ba atoms are shown in medium-green, the Bi atoms are in orange, the Li atoms in tetrahedral coordination are drawn in yellow (Li1 and Li3, remnants of the "1-3-2" slab) and light blue (Li2, remnants of the "3-4-4" slab), while the Li atoms in octahedral coordination are depicted in light-green. (**b**) Ball-and-stick representation of the same structure in the same projection.

Table 4. Selected distances (Å) in crystal structures of the "4-7-6" family of pnictides [a].

Atom Pair	$Ba_4(Li_{1-x}Ga_x)_7Sb_6$	$Ba_4(Li_{1-x}In_x)_7Sb_6$	$Ba_4(Li_{1-x}In_x)_7Bi_6$	$Eu_4(Li_{1-x}In_x)_7Bi_6$
*AE*1–*Pn*1(2×)	3.5192(9)	3.5243(6)	3.5538(6)	3.3772(6)
*AE*1–*Pn*2(1×)	3.488(1)	3.4998(8)	3.5540(9)	3.4113(8)
*AE*1–*Pn*3(2×)	3.5058(9)	3.5040(6)	3.5444(6)	3.3394(6)
*AE*1–*Pn*3(1×)	3.552(1)	3.5272(8)	3.5801(9)	3.3726(8)
*AE*2–*Pn*1(2×)	3.572(1)	3.5762(7)	3.6487(6)	3.5208(7)
*AE*2–*Pn*1(2×)	3.563(1)	3.5592(6)	3.6301(6)	3.4851(7)
*AE*2–*Pn*2(2×)	3.5556(9)	3.5682(6)	3.6195(6)	3.4671(6)
*Pn*1–*Pn*1(1×)	2.843(1)	2.847(1)	3.0589(9)	3.052(1)
Li1–*Pn*1(1×)	3.036(1)	3.09(1)	3.06(2)	2.95(2)
Li1–*Pn*2(1×)	2.961(1)	2.98(1)	3.07(2)	2.99(2)
Li1–*Pn*3(2×)	2.851(7)	2.844(6)	2.896(9)	2.799(9)
Li2–*Pn*1(1×)	2.96(1)	2.96(1)	3.00(2)	2.99(3)
Li2–*Pn*2(2×)	2.915(7)	2.913(7)	2.977(9)	2.84(1)
Li2–*Pn*2(1×)	3.00(1)	3.00(1)	2.99(2)	2.87(3)
Li3–*Pn*3(2×) [b]	2.812(4)	2.857(2)	2.930(3)	2.866(4)
Li3–*Pn*2(2×) [b]	2.977(2)	3.027(1)	3.071(2)	2.990(3)
Li4–*Pn*2(2×)	3.317(1)	3.3662(7)	3.4419(5)	3.3222(7)
Li4–*Pn*3(2×)	3.3468(8)	3.3842(5)	3.4407(4)	3.3827(5)

[a] The shown metrics are those from the refinements of $Ba_4Li_{6.55}Ga_{0.45(1)}Sb_6$, $Ba_4Li_{6.45}In_{0.55(1)}Sb_6$, $Ba_4Li_{6.45}In_{0.55(1)}Bi_6$, and $Eu_4Li_{6.60}In_{0.40(1)}Bi_6$, respectively. [b] Li3 is mixed-occupied with Ga or In.

Overall, all bonds are slightly lengthened in the structure with the larger cell volume, $Eu_4Li_{6.60}In_{0.40(1)}Bi_6$, but identifying the most affected bonds is challenging, as many of the changes are within 3–5 e.s.d.s. For example, the Bi_2 dumbbells elongate by 0.006(1) Å. Li–Bi interactions in the tetrahedral coordination are the ones that appear to show some statistically significant changes, which are mostly evident from the changes in bond angles. Focusing on the Li3 site, where the In substitution occurs, one can notice that while $d_{Li3-Bi3}$ = 2.866(4) Å/$d_{Li3-Bi2}$ = 2.990(3) Å in $Eu_4Li_{6.60}In_{0.40(1)}Bi_6$ are similar to $d_{Li3-Bi3}$ = 2.86(3) Å/$d_{Li3-Bi2}$ = 2.92(1) Å in $Eu_4Li_7Bi_6$, the Bi2–Li3–Bi2 bond angles are slightly different, 107.5(1)° for the former structure and 111.0(8)° for the latter, meaning a slightly different type of tetrahedral distortion in either case.

2.2. Crystal Structure and Bonding in $Ba_7Li_{11}Bi_{10}$

The new compound, $Ba_7Li_{11}Bi_{10}$, was discovered and synthesized for the first time from stoichiometric reactions of the elements as part of this study. $Ba_7Li_{11}Bi_{10}$ crystallizes with its own structure type, the Pearson index *mS*56 (Table 5). It is structurally related to the aforementioned "4-7-6" structures, which have 9 independent atomic positions (four for alkaline/rare-earth metals, three for the pnictogen atoms, and four for lithium atoms) in the asymmetric unit, while the $Ba_7Li_{11}Bi_{10}$ structure has 15 symmetry-unique positions (four for barium atoms, five for the bismuth atoms, and six for lithium atoms) in the asymmetric unit. The Wyckoff sequence for this new crystallographic arrangement is *i*13 *d a*. Consequently, the structure is rather complex (Figure 2). A common trait is shared between the $Ba_4(Li_{1-x}In_x)_7Bi_6$ and $Ba_7Li_{11}Bi_{10}$ structures. They both have anionic substructures based on isolated Bi^{3-} ions and $[Bi_2]^{4-}$ dimers. The positions of the Li atoms in the two structures are such that the $LiBi_4$ tetrahedra have similar connectivity, and the interatomic distances are closely matching (Tables 4 and 6).

Table 5. Selected crystal structure data refinement parameters for $Ba_7Li_{11}Bi_{10}$.

Empirical Formula	$Ba_7Li_{11}Bi_{10}$	$Ba_7Li_{11}Bi_{10}$	$Ba_7Li_{10.95}Ga_{0.05(2)}Bi_{10}$
Formula weight, g·mol^{-1}	3127.52	3127.52	3130.66
Space group, *Z*		*C*2/*m* (No.12), 2	
λ, Å		0.71073	
T, K		200(2)	
a, Å	18.407(3)	18.397(2)	18.407(4)
b, Å	5.0258(9)	5.0247(6)	5.0241(11)
c, Å	18.353(3)	18.345(2)	18.349(4)
β, °	104.426(3)	104.417(2)	104.395(3)
V, Å^3	1644.3(5)	1642.4(3)	1643.6(6)
ρ_{calc}, g·cm^{-3}	6.32	6.32	6.33
$\mu_{Mo\ K\alpha}$, cm^{-1}	614.9	615.7	615.6
Collected/independent reflections	9394/2063	10342/1753	12318/2061
R_{int}	0.0414	0.0484	0.0608
GOF on F^2	1.054	1.062	1.035
R_1 ($I > 2\sigma(I)$) [a]	0.0298	0.0299	0.0312
R_1 (all data) [a]	0.0399	0.0402	0.0400
wR_2 ($I > 2\sigma(I)$) [a]	0.0625	0.0606	0.0701
wR_2 (all data) [a]	0.0651	0.0659	0.0736
Largest peak/hole, e^- Å^{-3}	3.64/−2.69	5.85/−2.72	2.43/−2.58

[a] $R_1 = \sum||F_o| - |F_c||/\sum|F_o|$; $wR_2 = [\sum[w(F_o^2 - F_c^2)^2]/\sum[w(F_o^2)^2]]^{1/2}$, where $w = 1/[\sigma^2F_o^2 + (AP)^2 + (BP)]$, and $P = (F_o^2 + 2F_c^2)/3$; *A*, *B* are the respective weight coefficients (see CIF in the supporting information). A CIF has been deposited with reference number CSD 1867169.

The observed average Li–Bi distances range between 2.799(9) Å to 3.071(2) Å, and 2.96(3) Å to 3.10(2) Å, for the $Ba_4(Li_{1-x}In_x)_7Bi_6$ and $Ba_7Li_{11}Bi_{10}$ structures, respectively. These values are in close range with the sum of the Pauling covalent radii; $r_{Li} + r_{Bi}$ = 1.225 Å + 1.510 Å [24], as well as with those

reported for other compounds [13,20,27–29]. The tetrahedra are slightly distorted in both structures with the values for the Bi1–Li1–Bi2/Bi1–Li2–Bi3 bond angles ranging between 104.7(4)° and 111.8(3)°.

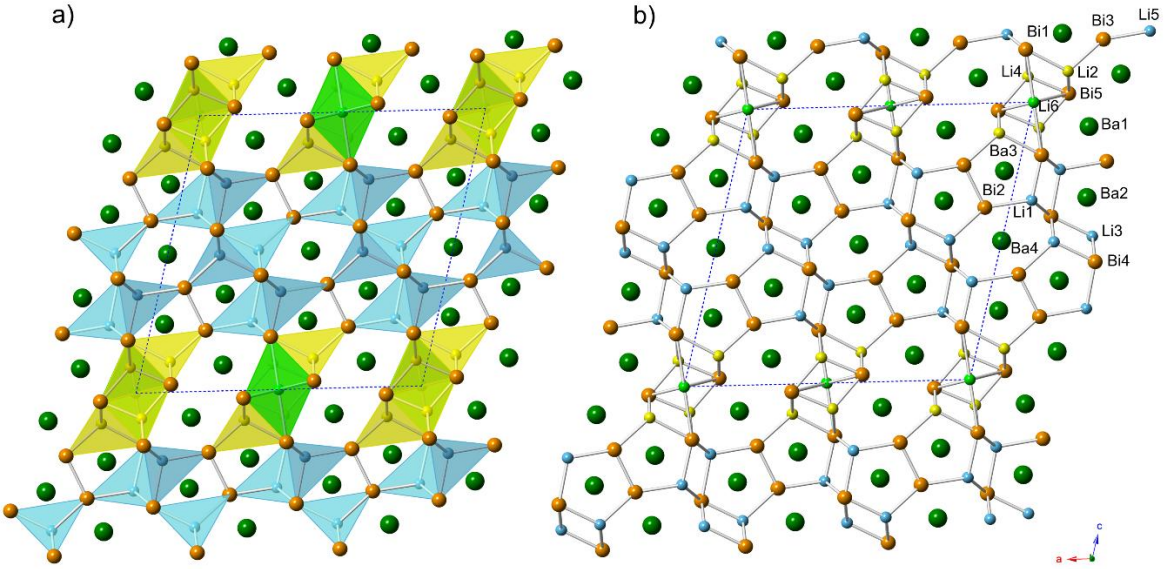

Figure 2. (**a**) Polyhedral representation of the crystal structure of $Ba_7Li_{11}Bi_{10}$, viewed down the crystallographic *b*-axis. Color codes of the atoms are the same as in Figure 1. (**b**) Ball-and-stick representation of the same structure in the same projection. The unit cell is outlined.

Table 6. Selected distances (Å) in $Ba_7Li_{11}Bi_{10}$.

Atom Pair	Distance	Atom Pair	Distance
Ba1–Bi1(1×)	3.569(1)	Li1–Bi1(1×)	2.96(3)
Ba1–Bi3(2×)	3.5611(8)	Li1–Bi2(1×)	3.08(3)
Ba1–Bi5(2×)	3.5432(8)	Li2–Bi1(1×)	3.04(3)
Ba1–Bi5(1×)	3.592(1)	Li2–Bi3(1×)	3.06(3)
Ba2–Bi2(2×)	3.6552(8)	Li3–Bi2(1×)	3.03(3)
Ba2–Bi3(2×)	3.6490(9)	Li3–Bi4(2×)	3.00(2)
Ba2–Bi4(2×)	3.6202(8)	Li4–Bi1(2×)	3.08(1)
Ba3–Bi1(2×)	3.6063(8)	Li4–Bi5(1×)	2.84(2)
Ba3–Bi2(2×)	3.6726(9)	Li4–Bi5(1×)	2.90(2)
Ba3–Bi3(2×)	3.6538(8)	Li5–Bi1(2×)	2.94(1)
Ba4–Bi2(4×)	3.4850(5)	Li5–Bi3(1×)	3.10(2)
Ba4–Bi4(2×)	3.5603(7)	Li6–Bi1(1×)	3.4398(8)
Bi2–Bi3(1×)	3.0443(8)	Li6–Bi5(2×)	3.4274(6)

Similar arguments used above can be applied to the $LiBi_6$ octahedra, where the average Li–Bi bond distances in the $Ba_4(Li_{1-x}In_x)_7Bi_6$ and $Ba_7Li_{11}Bi_{10}$ structures range between 3.4419(5) Å and 3.4407(4) Å for the former, and between 3.4274(6) Å and 3.4398(8) Å for the latter. In general, the bond lengths in the octahedra are longer than those in tetrahedral, as expected. The lengths of the Bi–Bi bonds in the $Ba_4(Li_{1-x}In_x)_7Bi_6$ and $Ba_7Li_{11}Bi_{10}$ structures match within two e.s.d.s.

2.3. Structural Relationships

Considering the similarities between the "4-7-6" and "7-11-10" structures, it can be proposed that the two are members of a homologous series. Let us illustrate this idea by taking two compounds with known structures—$Ba_3Li_4Bi_4$ ($Zr_3Cu_4Si_4$ structure type, Pearson symbol *oI*44) and $BaLi_3Bi_2$ ($LaLi_3Sb_2$ structure type, filled version of the $CaAl_2Si_2$ structure type, Pearson symbol *hP*6). We draw attention to the fact that the existence of the former compound has been experimentally confirmed, but the latter is not known. For electronic stability reasons, as discussed in the next section, $BaLi_3Bi_2$ is not

likely to form, and its closest analog would be $EuLi_{2.58}In_{0.42(2)}Bi_2$, which was obtained as a part of this study (see the Supplementary Materials). For comparison, the isotypic lanthanide-based $RELi_3Bi_2$ are valance-precise semiconductors, whose formulae can be represented as $(RE^{3+})(Li^{1+})_3(Bi^{3-})_2$, and they can be readily made [31]). Nonetheless, for the purposes of this discussion, $BaLi_3Bi_2$, even as a hypothetical case, will be considered, and slabs cut out from $Ba_3Li_4Bi_4$ and $BaLi_3Bi_2$ can be integrated to form $Ba_4Li_7Bi_6$ following Equation (1):

$$Ba_3Li_4Bi_4 + BaLi_3Bi_2 = Ba_4Li_7Bi_6 \quad (1)$$

A detailed description of the structural relationships that equation 1 describes is already discussed in the literature [13]. Now, using the same two fragments, the structure of $Ba_7Li_{11}Bi_{10}$ can be seen as realized through Equation (2):

$$2 \times Ba_3Li_4Bi_4 + BaLi_3Bi_2 = Ba_7Li_{11}Bi_{10} \quad (2)$$

In other words, $Ba_4Li_7Bi_6$ and $Ba_7Li_{11}Bi_{10}$ are the simplest members of the family described with the general formula $(BaLi_3Bi_2)_n(Ba_3Li_4Bi_4)_m$, where the $Ba_4Li_7Bi_6$ is the member with $n = 1$ and $m = 1$, and $Ba_7Li_{11}Bi_{10}$ is the intergrowth of the two components with $n = 1$ and $m = 2$, respectively. A pictorial representation of this analogy is shown in Figure 3.

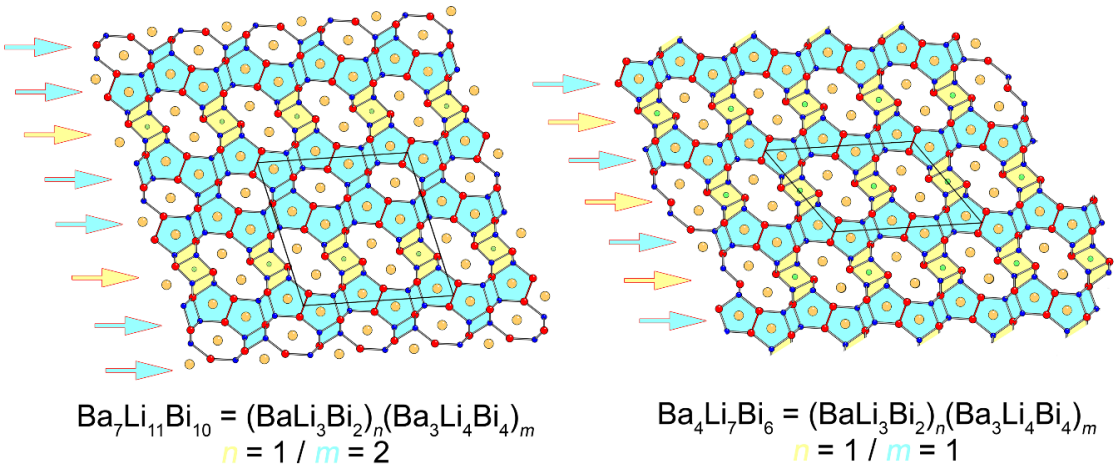

Figure 3. Schematic illustration of the structural relationship between $Ba_7Li_{11}Bi_{10}$ and $Ba_4Li_7Bi_6$, which are considered as intergrowths of the same type of fragments. The slabs cut out from $Ba_3Li_4Bi_4$ ($Zr_3Cu_4Si_4$ structure type) are highlighted in light-blue, and the slabs derived from $BaLi_3Bi_2$ ($LaLi_3Sb_2$ structure type) are highlighted in yellow.

The illustrated idea allows for the prediction of other possible members. For example, switching the ratio, i.e., taking the two components with $n = 2$ and $m = 1$, leads to $Ba_5Li_{10}Bi_8 = (BaLi_3Bi_2)_2(Ba_3Li_4Bi_4)_1$. Going above and beyond, based on this, one can envision the existence of other higher-order analogs such as $Ba_6Li_{13}Bi_{10}$ ($n = 3$ and $m = 1$) or $Ba_{10}Li_{15}Bi_{14}$ ($n = 1$ and $m = 3$). Experiments aimed at making these compounds were attempted, but so far they have been unsuccessful.

Another interesting structural relationship that can be mentioned here concerns the similarities between the structure of $Ba_4Li_7Bi_6$ and that of $Ba_4Cd_4Bi_6$ (=$Ba_2Cd_2Bi_3$), which is actually not reported yet, but presumed to be isotypic with $Ba_2Cd_2Sb_3$ (own type with the monoclinic space group $C2/m$ and Pearson symbol $mS28$) [32]. The latter structure is described as a derivative of $BaCd_2Sb_2$ with the $CaAl_2Si_2$ structure type. Recall that the $BaLi_3Bi_2$ compound that we considered in our homologous series is the same basic structure, where an extra Li atom is inserted within. Given that Cd is nominally divalent, one can reason that the very same structure that is adopted by the Cd-bearing compound cannot be realized if Li (nominally monovalent) is used. Instead, the $Ba_2Li_2Bi_3$ sub-structure can be

seen as being distorted a little around the pivotal Bi_2-dimers, which creates two more tetrahedral holes that are suitable for Li (described by one crystallographic position, Li2 in the notation used for the "4-7-6" structures—Figure 1). Still two electrons short of the ideal number of valence electrons, the imaginary $Ba_4Li_6Bi_6$ accepts one more Li atom, in an octahedral hole (described by position Li4 in the notation used for the "4-7-6" structures). A pictorial representation of this analogy is shown in Figure 4.

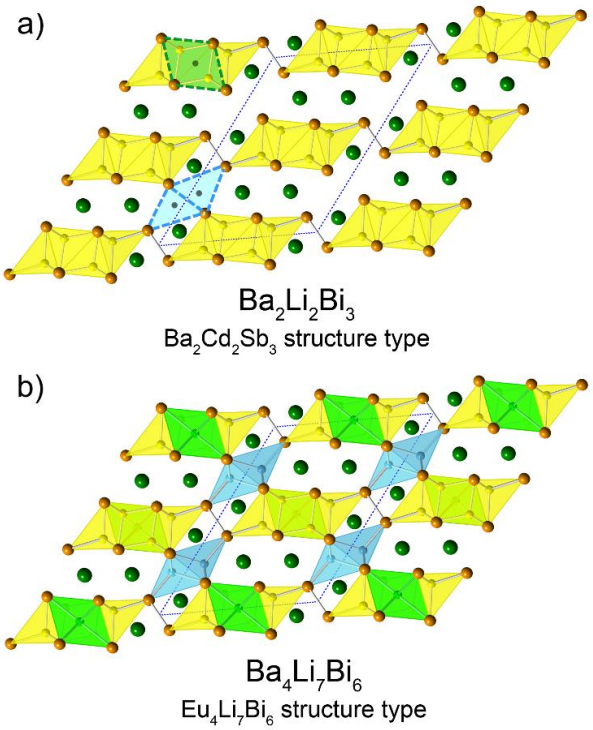

Figure 4. Schematic illustration of the structural relationship between the $Ba_2Cd_2Sb_3$ (**a**) and $Eu_4Li_7Bi_6$ (**b**) structure types, which both crystallize in the same monoclinic space group $C2/m$. The three "empty" holes in imaginary $Ba_4Li_4Bi_6$ (=$Ba_2Li_2Bi_3$) that can be filled with Li atoms to yield $Ba_4Li_7Bi_6$ are emphasized. Octahedral positions are in green, tetrahedral ones are in light-blue, in accordance with the color coding for the other figures.

2.4. Valence Electron Count and Electronic Band Structure

As mentioned earlier in this paper, $Eu_4Li_7Bi_6$ does not appear to satisfy the Zintl–Klemm electron counting scheme [33], as attempts to rationalize the structure ($(Eu^{2+})_4(Li^+)_7([Bi_2]^{4-})(Bi^{3-})_4(h^+)$, where h^+ denotes an electron hole) fail to produce a charge-balanced formula [13]. In other words, the compound $Eu_4Li_7Bi_6$, joins the ranks of electron-deficient "near" Zintl phases, such as the families of $Ca_{14}MnBi_{11}$ [34] and $Ca_9Zn_4Sb_9$ [35]. The structure of the former has been experimentally confirmed to contain an electron hole, and it can be judiciously tuned to a Zintl phase by the aliovalent substitution of one Ca^{2+} cation by one RE^{3+} cation (*RE* = rare-earth metal), as demonstrated with the examples of $Ca_{13}REMnBi_{11}$ [36] and $Ca_{13}REMnSb_{11}$ [37]. On the other hand, the originally published $Ca_9Zn_4Sb_9$ structure has been revisited, and an interstitial position within it has been identified, i.e., the formula is $Ca_9Zn_{4+x}Sb_9$ [38], which also brings the valence electron count very close to the expected from the Zintl concept. This structure has also been shown to be amenable to tuning via substitution, as demonstrated with the example of $Ca_8REMn_4Sb_9$ [39], where the interstitial site is empty, but the electron count is modulated by the extra electron contributed by the rare-earth metal substituting for Ca.

On the opposite side of the spectrum, here are some nominally Zintl phases with the "wrong" electron count. Good examples are the structures of Ca_4Bi_2O (previously thought to be Ca_2Bi) [40], and the unusual $Ba_5Cd_2Sb_5O_{0.5}$ [41]. For both of them, the perceived electron surplus has helped

to identify the unrecognized oxygen impurity. Considering the ambivalent role that Li can play in intermetallics, we might bring up the case studies carried out on germanides/stannide with complex structures, such as $AELi_{1-x}In_xGe_2$, $RE_4Li_{4-x}Sn_{4+x}$ and $Li_{9-x}EuSn_{6+x}$ [14–16], which show the tendency of such structures to attain more optimal valence electron counts by Li-group 13 or Li-group 14 element substitutions.

Armed with the knowledge from the above-mentioned studies, we considered many different hypotheses, to ultimately settle on the notion that the electron count for the "4-7-6" compounds needs to be augmented, which is achieved by virtue of substituting a fraction of the Li atoms with either Ga or In atoms. As seen from the total and partial density of states (DOS) curves of $Ba_4Li_7Bi_6$ (Figure 5), the integrated DOS at the Fermi level (E_F = 0 eV) corresponds to 45 valence electrons per unit cell. Note that the calculation is done on $Ba_4Li_7Bi_6$, which is an ordered model of the actual $Ba_4(Li_{1-x}In_x)_7Bi_6$ structure, where the mixed occupied Li/In site, according to the single-crystal structure refinement data, were treated as only occupied by Li atoms. A closer inspection shows that an additional electron is required to reach the top of the valence band, in analogy to the findings previously discussed for $Eu_4Li_7Bi_6$ [13]. Thus, the electronic calculations are in excellent agreement with the formulation based on the Zintl–Klemm concept. Given the inability to prepare other pure ternary compounds with this structure with Ba or Sr, both of which can contribute only two electrons to the bonding, it can be surmised that the hypothetical $Ba_4Li_7Bi_6$ cannot be realized, and that Ga or In doping on the Li site is critical to obtain more electronically stable, charge-balanced compounds.

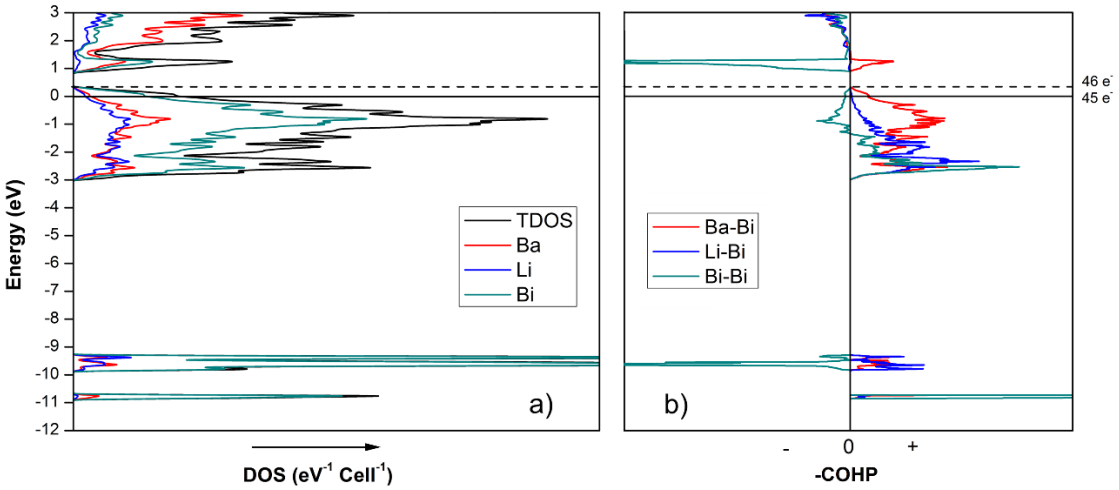

Figure 5. (**a**) Projected total and partial density of states (DOS) for $Ba_4Li_7Bi_6$. The partial DOS curves illustrate the contribution of different atoms to the total DOS (E_F = 0 eV). (**b**) Crystal orbital Hamilton population (COHP) plots for Ba–Bi, Li–Bi and Bi–Bi interactions shown on the same energy scale. The COHP values are inverted, which is done so that "−" and "+" denote the antibonding and bonding regions, respectively.

$Ba_7Li_{11}Bi_{10}$ is not an electron-precise compound either. According to Zintl concept, the empirical formula of $Ba_7Li_{11}Bi_{10}$ can be broken down to $(Ba^{2+})_7(Li^+)_{11}([Bi_2]^{4-})_2(Bi^{3-})_6(h^+)$, which indicates a shortage of one electron per formula unit. This is not surprising, given that the building blocks of $Ba_4Li_7Bi_6$ and $Ba_7Li_{11}Bi_{10}$ are the same (*vide supra*). The total and partial density of states (DOS) curves of $Ba_7Li_{11}Bi_{10}$ are shown in Figure 6, and agree with this conjecture—indeed, similar electronic characteristics can be noticed. For instance, both structures have non-zero DOS at the Fermi level, indicating metallic behavior. The *s* orbitals of Bi contribute almost exclusively to the energy DOS peaks in the −11 to −9.5 eV range, with the majority of them being lone pairs. Considering the very sharp bonding and antibonding peaks in the same energy range, as shown in the crystal orbital Hamilton population (COHP) in Figure 6b, the *s* orbitals of Bi are also responsible for the σ-bonding (and σ*-antibonding) states of the Bi_2-dimer. The *p* orbitals of Bi are mixed with Ba and Li orbitals

in the range between −3 eV to the Fermi level, suggesting the emergence of multiple covalent type interactions between these atoms.

The integrated DOS for $Ba_7Li_{11}Bi_{10}$ (Figure 6) at E_F = 0 eV corresponds to 75 valence electrons per unit cell. If the rigid band model is employed, integrating the DOS to 76 valence electrons, which is what the Zintl concept predicts, moves the Fermi level up in energy to a local DOS minimum at ca. 0.3 eV. This is perhaps the most notable difference between the electronic structures of $Ba_4Li_7Bi_6$ and $Ba_7Li_{11}Bi_{10}$, where an augmented electron count for the former leads to an electronic structure that is fully optimized, and a sizeable band-gap is opened, whereas for the latter, adding one more electron only helps to reach a nearly vanishing energy gap. This small difference might explain why doping in the $Ba_7Li_{11}Bi_{10}$ structure is not as critical as it is for the $Ba_4Li_7Bi_6$ counterpart, in line with the realization that, as discussed earlier, the $Ba_4Li_7Bi_6$ structure might be seen as being made up of 50% $BaLi_3Bi_2$-fragments, which are electron-deficient by nature. By comparison, in $Ba_7Li_{11}Bi_{10}$, the contribution of the electron-deficient $BaLi_3Bi_2$-component is reduced to one-third.

For a better understanding of the atomic interactions, the crystal orbital Hamilton population (COHP) curves were constructed and closely examined. In general, the bonding picture in herein is similar to what was previously described for the $Eu_4Li_7Bi_6$ compound [13]. The bonding description here is valid for both $Ba_4Li_7Bi_6$ and $Ba_7Li_{11}Bi_{10}$ compounds. The COHP curve of the Bi–Bi dimers show antibonding character close to the Fermi level in addition to some deeper bonding states. For both structures, the values for the integrated –COHP for Bi–Bi interactions are essentially the same at the Fermi level (~1.6 eV per bond). Although a direct comparison between the bonding strengths of different linear muffin-tin orbital (LMTO) calculations is not valid, we can see that the magnitude of the Bi–Bi bonding interactions is approximately the same. Judging from the –COHPs, the antibonding π* and σ* states of the $[Bi_2]$ dimers derived from p-orbitals are not completely occupied, which may indicate that the bond order within the dimers is not 1, like in the I_2 molecule to which an analogy was drawn earlier, but higher. The notion of a "double bond" is inconsistent with the lengths of the Bi–Bi bonds in both $Ba_4(Li_{1-x}In_x)_7Bi_6$ and $Ba_7Li_{11}Bi_{10}$ structures (Tables 4 and 6, respectively), but partial/non-integer bond order is conceivable. Thus, the formulae $Ba_4Li_7Bi_6$ and $Ba_7Li_{11}Bi_{10}$ can be formally represented as $(Ba^{2+})_4(Li^+)_7([Bi_2]^{3-}(Bi^{3-})_4$ and $(Ba^{2+})_7(Li^+)_{11}([Bi_2]^{3.5-})_2(Bi^{3-})_6$, respectively. In this view, the idealized "4-7-6" compounds will have a higher bond order (i.e., 1.5) tan the "7-11-10" ones, but this difference is offset in the actual "4-7-6" compounds by the partial substitution of In or Ga for Li; hence, the formal charge of the $[Bi_2]$ moieties in both is about the same.

The Li–Bi bonds are optimized, reflecting the strong covalent nature, while the Ba–Bi interactions are slightly underoptimized (electron-deficient) because there are still bonding states available above the Fermi level. This situation will not change even by adding more electrons, i.e., moving the Fermi level up to the gap. This scenario is not unusual for highly polar interactions with strong ionic contribution [42]. Similarly, the Li–Bi will not change much if the Fermi level were shifted up because only a few states are available above the Fermi level and are of anti-bonding character for the Bi–Bi interactions and bonding for Li–Bi ones. We can estimate that for both structures, the integrated –COHP values for the Li–Bi interactions lie between 0.1 and 0.4 eV per bond, while for the Ba–Bi interactions, they range between 0.4 and 0.7 eV per bond.

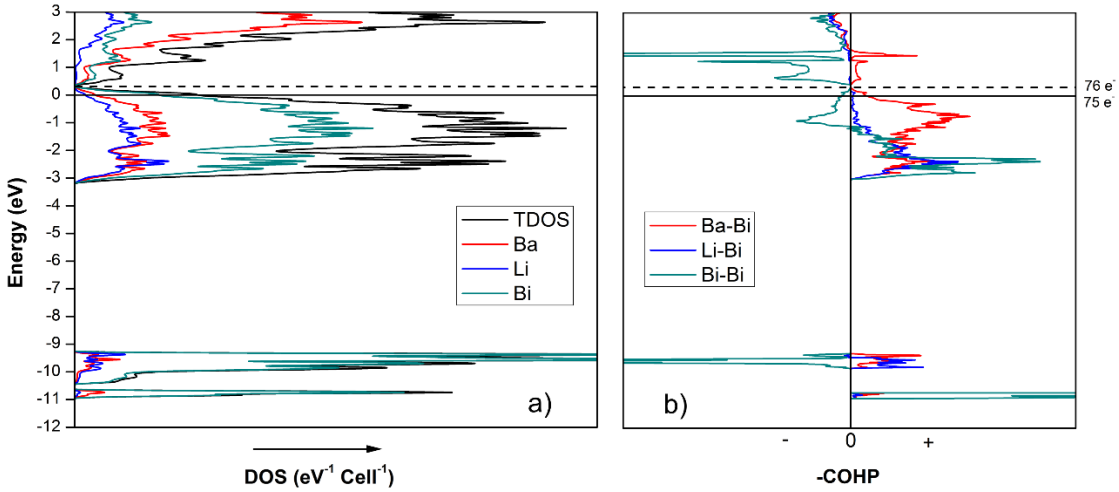

Figure 6. (**a**) Projected total and partial DOS for $Ba_7Li_{11}Bi_{10}$. The partial DOS curves illustrate the contribution of different atoms to the total DOS (E_F = 0 eV). (**b**) The reversed COHP plots for Ba–Bi, Li–Bi and Bi–Bi interactions shown on the same energy scale.

3. Materials and Methods

3.1. Synthesis

Owing to their air-sensitivity, all of the starting materials and products were manipulated and stored in an Ar-filled glovebox (H_2O, <1 ppm; O_2, <1 ppm) or under a vacuum. All of the reagents had purities of greater than 99.9 wt %, and they were used as purchased from Sigma-Aldrich (Saint Louis, MO, USA) or Alfa Aesar (Tewksbury, NJ, USA). The surfaces of the lithium and barium rods were scraped clean before use. For direct solid-state reactions, mixtures of the starting elements in the desired stoichiometric ratios were weighed (~500 mg) and loaded into Nb tubes, arc-welded under an Ar atmosphere, and enclosed in evacuated fused silica ampoules to prevent oxidation upon heating to high temperatures. The reaction vessels were placed in high-temperature tube-furnaces with programmable controllers (Thermo Fisher Scientific, Waltham, MA, USA). Many batches of $AE_4(Li_{1-x}Ga_x)_7Pn_6$ and $AE_4(Li_{1-x}In_x)_7Pn_6$ (AE = Sr, Ba, Eu; Pn = Sb, Bi) samples were prepared with varied Li/Ga and Li/In ratios. From one such reaction aimed at $Ba_4(Li_{1-x}Ga_x)_7Bi_6$, a compound with a new structure was identified, that of $Ba_7Li_{11}Bi_{10}$. After the structure and composition were established, experiments were set up to make isotypic $Ba_7Li_{11}Sb_{10}$, as well as $AE_7Li_{11}Sb_{10}$ and $AE_7Li_{11}Bi_{10}$ (AE = Sr, Eu), but they were not successful.

For all of the reported compounds, the reaction products were multi-phase mixtures, and therefore they could not be used for property measurements. Attempts to optimize the conditions for preparing the target compounds were made of course—in each system, several experiments with different temperature profiles were explored. The best synthesis route involved ramping the temperature to 860 °C at a rate of 300 °C/h, and then holding the temperature for 48 h, during which period, the ampoules were turned by hand several times to ensure sample homogeneity. The reaction mixtures were slowly cooled down to ambient temperature at a rate of −4 °C/h. The Nb tubes were brought into the glovebox and cut open. The typical products formed were polycrystalline, which under an inspection by optical microscope were seen to contain small irregularly-shaped crystals with silver luster. The polycrystalline materials are air-sensitive and samples left exposed to air were visually found to decompose within 24 h or less.

All reported structures were established by single-crystal X-ray crystallography. We need to mention here that almost all structurally characterized "4-7-6" samples are Ba-containing phases, and one contains Eu. There are no refined structures with Sr, although many specimens were prepared, but the crystals' quality was inadequate for structure solution and refinement. For example, based on

the obtained unit cell volume and partial structure solution, we are confident that $Sr_4(Li_{1-x}Ga_x)_7Bi_6$ also exists (a = 17.750(7) Å, b = 4.846(2) Å, and c = 12.910(5) Å, β = 125.93(1)°). Note that since Sr^{2+} and Eu^{2+} have almost identical effective ionic sizes [30], the unit cell parameters of the structurally characterized $Eu_4(Li_{1-x}In_x)_7Bi_6$ (a = 17.642(4) Å, b = 4.8297(10) Å, and c = 12.850(3) Å, β = 125.85(1)°) are a very close match to those of the speculated $Sr_4(Li_{1-x}Ga_x)_7Bi_6$.

In the course of the study, several other new phases were serendipitously encountered. These include BaLiBi, $Ba(Li_{1-x}In_x)_2Bi_2$, $Sr_3Li_3GaSb_4$, $Sr_3Li_3InSb_4$, and $Eu(Li_{1-x}In_x)Li_2Bi_2$, among others that are still unknown. Structural work to fully elucidate the structures of the above-mentioned compounds is ongoing. Preliminary data for $Eu(Li_{1-x}In_x)Li_2Bi_2$ (isotypic to $LaLi_3Sb_2$, a "filled" variant of the $CaAl_2Si_2$-type) is given as Supplementary Materials, since this structure is a building block of the herein discussed "4-7-6" and "7-11-10" structures.

3.2. Powder X-Ray Diffraction

Room-temperature powder X-ray diffraction (PXRD) patterns of the raw reaction products were recorded in Bragg–Brentano geometry by the means of a Rigaku MiniFlex powder diffractometer (Rigaku Corporation, Tokyo, Japan) using nickel-filtered Cu Kα (λ = 1.5418 Å) radiation. Powder diffractograms were recorded in the 2θ range 5–75°, with a step size of 0.05° and 2 s/step counting time. The diffractometer was operated inside a nitrogen-filled glovebox to allow for data collection of air-sensitive samples. The collected powder X-ray diffraction patterns were only used to check the phase purity. This was performed using a *JADE* 6.5 software package (MDI, Livermore, CA, USA). Structure elucidation was done by means of single-crystal X-ray diffraction methods.

3.3. Single-Crystal X-Ray Diffraction

Single-crystal X-ray diffraction data were collected on a Bruker APEX-II CCD-based diffractometer with graphite-monochromated Mo Kα (λ = 0.71073 Å) radiation equipped with a low-temperature apparatus (Bruker AXS, Madison, WI, USA). The measurements were carried out at a steady temperature of 200 K. Prior to the data collection, a few crystals were selected from each sample batch, cut in Paratone N oil to the desired dimensions, mounted on glass fibers, and checked for quality. The program Bruker *APEX2* was used for data collection, while cell refinement and data reduction were performed using the Bruker *SAINT* program [43]. Semi-empirical absorption correction based on equivalent reflections was applied with *SADABS* [44]. The structures were solved by the *SHELXS* structure solution program using direct methods, while the refinements were performed by *SHELXL* using least-squares minimization [45,46]. Atomic coordinates were standardized using the *STRUCTURE TIDY* program [47]. The final positional coordinates and displacement parameters from all refined structures are displayed in Tables 7 and 8.

Table 7. Final refined positional coordinates and displacement parameters for $AE_4(Li_{1-x}Ga_x)_7Pn_6$ and $AE_4(Li_{1-x}In_x)_7Pn_6$ (*AE* = Ba, Eu; *Pn* = Sb, Bi). The shown metrics are those from the refinements of $Ba_4Li_{6.55}Ga_{0.45(1)}Sb_6$, $Ba_4Li_{6.45}In_{0.55(1)}Sb_6$, $Ba_4Li_{6.45}In_{0.55(1)}Bi_6$, and $Eu_4Li_{6.60}In_{0.40(1)}Bi_6$, respectively.

Atom	Wyckoff Site	x	y	z	U_{iso} [a]/U_{eq}, [b] Å^2	Occupancy
			$Ba_4(Li_{1-x}Ga_x)_7Sb_6$			
Ba1	4*i*	0.2613(1)	0	0.6602(1)	0.0108(2)	1
Ba2	4*i*	0.4295(1)	0	0.0856(1)	0.0119(1)	1
Sb1	4*i*	0.0856(1)	0	0.1241(1)	0.0100(2)	1
Sb2	4*i*	0.1580(1)	0	0.8152(1)	0.0134(2)	1
Sb3	4*i*	0.3973(1)	0	0.5455(1)	0.0124(2)	1
Li1	4*i*	0.0435(1)	0	0.318(1)	0.007(1) [a]	1
Li2	4*i*	0.2340(9)	0	0.094(1)	0.007(1) [a]	1
Li3/Ga	4*i*	0.4136(3)	0	0.3444(4)	0.007(1) [a]	0.833(4)/0.167
Li4	2*c*	0	0	$\frac{1}{2}$	0.019(5)	1

Table 7. *Cont.*

Atom	Wyckoff Site	x	y	z	U_{iso} [a]/U_{eq}, [b] Å^2	Occupancy
			$Ba_4(Li_{1-x}In_x)_7Sb_6$			
Ba1	4*i*	0.2615(1)	0	0.6602(1)	0.0118(1)	1
Ba2	4*i*	0.4295(1)	0	0.0856(1)	0.0119(1)	1
Sb1	4*i*	0.0854(1)	0	0.1238(1)	0.0105(1)	1
Sb2	4*i*	0.1599(1)	0	0.8185(1)	0.0126(1)	1
Sb3	4*i*	0.3949(1)	0	0.5457(1)	0.0118(1)	1
Li1	4*i*	0.0429(8)	0	0.320(1)	0.013(2) [a]	1
Li2	4*i*	0.2340(9)	0	0.094(1)	0.016(3) [a]	1
Li3/In	4*i*	0.4144(1)	0	0.3583(2)	0.0144(6) [a]	0.712(2)/0.288
Li4	2*c*	0	0	$\frac{1}{2}$	0.045(6) [a]	1
			$Ba_4(Li_{1-x}In_x)_7Bi_6$			
Ba1	4*i*	0.2596(1)	0	0.6588(1)	0.0196(2)	1
Ba2	4*i*	0.4301(1)	0	0.0844(1)	0.0192(2)	1
Bi1	4*i*	0.0898(1)	0	0.1302(1)	0.0184(1)	1
Bi2	4*i*	0.1590(1)	0	0.8191(1)	0.0199(2)	1
Bi3	4*i*	0.3942(1)	0	0.5455(1)	0.0199(2)	1
Li1	4*i*	0.046(1)	0	0.319(2)	0.007(2) [a]	1
Li2	4*i*	0.233(1)	0	0.089(2)	0.007(2) [a]	1
Li3/In	4*i*	0.4135(2)	0	0.3466(3)	0.023(1) [a]	0.770(4)/0.230
Li4	2*c*	0	0	$\frac{1}{2}$	0.07(1) [a]	1
			$Eu_4(Li_{1-x}In_x)_7Bi_6$			
Eu1	4*i*	0.2598(1)	0	0.6626(1)	0.0144(2)	1
Eu2	4*i*	0.4328(1)	0	0.0855(1)	0.0155(2)	1
Bi1	4*i*	0.0933(1)	0	0.1334(1)	0.0131(1)	1
Bi2	4*i*	0.1557(1)	0	0.8181(1)	0.0147(1)	1
Bi3	4*i*	0.3831(1)	0	0.5375(1)	0.0148(1)	1
Li1	4*i*	0.053(1)	0	0.3259(5)	0.004(4) [a]	1
Li2	4*i*	0.239(2)	0	0.089(2)	0.021(1) [a]	1
Li3/In	4*i*	0.4205(3)	0	0.3521(4)	0.021(2) [a]	0.802(5)/0.198
Li4	2*c*	0	0	$\frac{1}{2}$	0.06(2) [a]	1

[a] Isotropic refinement. [b] U_{eq} is defined as one third of the trace of the orthogonalized U_{ij} tensor.

Table 8. Final refined positional coordinates and displacement parameters for $Ba_7Li_{11}Bi_{10}$.

Atom	Wyckoff Site	x	y	z	U_{iso} [a]/U_{eq}, [b] Å^2	Occupancy
Ba1	4*i*	0.2149(1)	0	0.0934(1)	0.0102(2)	1
Ba2	4*i*	0.2649(1)	0	0.3502(1)	0.0105(2)	1
Ba3	4*i*	0.4538(1)	0	0.2467(1)	0.0099(2)	1
Ba4	2*d*	0	$\frac{1}{2}$	$\frac{1}{2}$	0.0093(2)	1
Bi1	4*i*	0.0705(1)	0	0.1921(1)	0.0100(1)	1
Bi2	4*i*	0.0866(1)	0	0.6228(1)	0.0091(1)	1
Bi3	4*i*	0.1945(1)	0	0.7783(1)	0.0097(1)	1
Bi4	4*i*	0.3455(1)	0	0.5843(1)	0.0099(1)	1
Bi5	4*i*	0.3833(1)	0	0.0282(1)	0.0103(1)	1
Li1	4*i*	0.073(1)	0	0.354(1)	0.015(5) [a]	1
Li2	4*i*	0.095(2)	0	0.889(2)	0.023(6) [a]	1
Li3	4*i*	0.180(1)	0	0.508(2)	0.018(6) [a]	1
Li4	4*i*	0.540(1)	0	0.092(1)	0.006(3) [a]	1
Li5	4*i*	0.646(1)	0	0.249(1)	0.006(3) [a]	1
Li6	2*a*	0	0	0	0.006(3) [a]	1

[a] Isotropic refinement. [b] U_{eq} is defined as one third of the trace of the orthogonalized U_{ij} tensor.

Multiple data collections and structure solution and refinements were carried out, in part, to ensure reproducibility, and in part, as a result of some problems with refining the displacement parameters and/or occupation factors of the very light Li atoms, especially when the heavy Ba and Bi

are in near proximity. Specifically, the $Ba_4(Li_{1-x}Ga_x)_7Sb_6$, $Ba_4(Li_{1-x}In_x)_7Sb_6$, $Ba_4(Li_{1-x}In_x)_7Bi_6$, and $Eu_4(Li_{1-x}In_x)_7Bi_6$ structures have four crystallographically distinct sites, one of which is a special position. The $Ba_7Li_{11}Bi_{10}$ structure has two additional Li sites, six in total, and one of which is also on a special position with fixed coordinates. The refinement of the heavy elements in each case proceeded smoothly. However, refining the Li atoms, particularly when the refinements were attempted with anisotropic atomic displacement parameters proved difficult. Those problems are believed to originate from crystal quality issues and/or inadequate correction for absorption, as evidenced from the data gathered in Tables 2, 3 and 5. Therefore, in some refined structures, some or all Li atoms are refined with isotropic atomic displacement parameters; in some instances, to ensure convergence, constraints may have been applied as well. The site occupancy factors (SOF) for all of the atoms in each compound were refined independently to verify the presence/lack of crystallographic ordering, and in the cases of the "doped" $Ba_4(Li_{1-x}Ga_x)_7Sb_6$, $Ba_4(Li_{1-x}In_x)_7Sb_6$, $Ba_4(Li_{1-x}In_x)_7Bi_6$, and $Eu_4(Li_{1-x}In_x)_7Bi_6$, particular attention was paid to the SOFs of the Li positions. From the multiple refinements for crystals from different batches, it was established that the Li1, Li2, and Li4 positions in the structures of the above-mentioned compounds were fully occupied, while the Li3 positions revealed excess electron densities with SOFs often exceeding the scattering power of elemental Li by ca. 300–500%. The latter were treated as being mixed-occupied with In or Ga, and the refinement of structures from crystals selected from different batches revealed small compositional variations, concomitant with small changes in the unit cell constants, suggesting possible homogeneity ranges. Similar kinds of Li–In, Li–Ge, or Li–Sn disorder have been discussed in other publications [14–17,48].

The refinements of $Ba_7Li_{11}Bi_{10}$ (and its targeted Ga-doped version, Table 5) showed that the heavy atoms were well behaved, whereas at least three of the six crystallographic distinct Li sites exhibited problems—their thermal parameters could not be refined anisotropically in some cases, and in addition, there were high uncertainties, even when they were refined isotropically. The Li6 site (special position) showed an occupation factor exceeding unity (sometimes by almost 50–60%) when freed, even in the sample that was prepared from an elemental mixture of Ba, Li, and Bi only, i.e., it was not deliberately doped with Ga. Such presumed excess electron density on the Li6 site is very difficult to explain, and most likely due to inadequate crystal quality, as multiple data collections showed great variations in the refinements of all Li sites, and of Li6 in particular. This, combined with the fact that the unit cell volume appears to be invariant of the synthesis route, and that the changes upon the introduction of a dopant element are negligible, is indirect proof that the $Ba_7Li_{11}Bi_{10}$ structure is not as susceptible to alteration as the structures of $Ba_4(Li_{1-x}Ga_x)_7Sb_6$, $Ba_4(Li_{1-x}In_x)_7Sb_6$, $Ba_4(Li_{1-x}In_x)_7Bi_6$, and $Eu_4(Li_{1-x}In_x)_7Bi_6$.

CSD 1867165, 1867166, 1867167, 1867168 and 1867169 contain the supplementary crystallographic data for this paper. These data can be obtained free of charge via http://www.ccdc.cam.ac.uk/conts/retrieving.html (or from the CCDC, 12 Union Road, Cambridge CB2 1EZ, UK; Fax: +44 1223 336033; E-mail: deposit@ccdc.cam.ac.uk).

3.4. Electronic Structure Calculations

The electronic structure calculations for $Ba_4Li_7Bi_6$ and $Ba_7Li_{11}Bi_{10}$ compounds were performed using the tight-binding linear muffin-tin orbital (TB-LMTO) method with atomic spheres approximation (ASA), using the *TB-LMTO-ASA* 4.7 program [49]. The von Barth-Hedin LDA functional [50] was employed and the Brillouin zone was sampled by 78 and 310 *k*-points sets for the $Ba_4Li_7Bi_6$ and $Ba_7Li_{11}Bi_{10}$ structures, respectively. The density of states (DOS) and the crystal orbital Hamilton population (COHP) were evaluated using the automatic procedure in the LMTO code.

4. Conclusions

In the course of this study we discovered many new members of the series of compounds based on the "4-7-6" structure [13], as well as the novel compound $Ba_7Li_{11}Bi_{10}$. The "4-7-6" and "7-11-10"

structures are homologues, and can be formally considered as being built from the same building block. This modular approach can be further extended for other pnictides.

Supplementary Materials: The following are available online at http://www.mdpi.com/2304-6740/6/4/109/s1, Figure S1: Polyhedral representation of the crystal structure of $EuLi_{2.58}In_{0.42(2)}Bi_2$, Table S1: Selected crystal structure data and refinement parameters for $EuLi_{2.58}In_{0.42(2)}Bi_2$, Table S2: Final refined positional coordinates and displacement parameters for $EuLi_{2.58}In_{0.42(2)}Bi_2$, A combined CIF and checkCIF for all discussed structures.

Author Contributions: D.O.O., investigation; S.B., resources; D.O.O., writing—original draft preparation; S.B., writing—review and editing; S.B., supervision; S.B., project administration.

Funding: This research was funded by U.S. Department of Energy, Office of Science, Basic Energy Sciences, Award # DE-SC0008885.

Acknowledgments: We express gratitude to Yi Wang for the synthesis of some $Ba_4(Li_{1-x}In_x)_7Sb_6$ samples and Alexander Ovchinnikov for assistance with the electronic band structure calculations. The authors are also indebted to the anonymous reviewer who made very helpful suggestions regarding the interpretation of the computational results.

Conflicts of Interest: The authors declare no conflict of interest.

References

1. Snyder, G.J.; Toberer, E.S. Complex thermoelectric materials. *Nat. Mater.* **2008**, *7*, 105–114. [CrossRef] [PubMed]
2. Xu, Z.; Guloy, A.M. $Ca_5In_9Sn_6$: Interplay of structural and electronic factors between intermetallic and Zintl phases. *J. Am. Chem. Soc.* **1998**, *120*, 7349–7350. [CrossRef]
3. Chan, J.Y.; Kauzlarich, S.M.; Klavins, P.; Liu, J.; Shelton, R.N.; Webb, D.J. Synthesis, magnetic properties, and colossal magnetoresistance of $Eu_{13.97}Gd_{0.03}MnSb_{11}$. *Phys. Rev. B* **2000**, *61*, 459–463. [CrossRef]
4. Zevalkink, A.; Swallow, J.; Snyder, G.J. Thermoelectric properties of Zn-doped $Ca_5In_2Sb_6$. *Dalton Trans.* **2013**, *42*, 9713–9719. [CrossRef] [PubMed]
5. Park, S.-M.; Choi, E.S.; Kang, W.; Kim, S.-J. $Eu_5In_2Sb_6$, $Eu_5In_{2-x}Zn_xSb_6$: rare earth Zintl phases with narrow band gaps. *J. Mater. Chem.* **2002**, *12*, 1839–1843. [CrossRef]
6. Brown, S.R.; Kauzlarich, S.M.; Gascoin, F.; Snyder, J.G. $Yb_{14}MnSb_{11}$: New high efficiency thermoelectric material for power generation. *Chem. Mater.* **2006**, *18*, 1873–1877. [CrossRef]
7. Yan, Y.L.; Wang, Y.X.; Zhang, G.B. Electronic structure and thermoelectric performance of Zintl compound $Ca_5Ga_2As_6$. *J. Mater. Chem.* **2012**, *22*, 20284–20290. [CrossRef]
8. Zevalkink, A.; Toberer, E.S.; Bleith, T.; Flage-Larsen, E.; Snyder, G.J. Improved carrier concentration control in Zn-doped $Ca_5Al_2Sb_6$. *J. Appl. Phys.* **2011**, *110*, 013721. [CrossRef]
9. Makongo, J.P.A.; You, T.S.; He, H.; Suen, N.-T.; Bobev, S. New lithium-containing pnictides with 1-D infinite chains of supertetrahedral clusters: Synthesis, crystal and electronic structure of $Ba_4Li_2Cd_3Pn_6$ (*Pn* = P, As and Sb). *Eur. J. Inorg. Chem.* **2014**, *2014*, 5113–5124. [CrossRef]
10. Wang, Y.; Stoyko, S.; Bobev, S. Quaternary pnictides with complex, noncentrosymmetric structures. Synthesis and structural characterization of the new Zintl phases $Na_{11}Ca_2Al_3Sb_8$, $Na_4CaGaSb_3$, and $Na_{15}Ca_3In_5Sb_{12}$. *Inorg. Chem.* **2015**, *54*, 1931–1939. [CrossRef] [PubMed]
11. Xia, S.-Q.; Hullmann, J.; Bobev, S. Gallium substitutions as a means to stabilize alkaline-earth and rare-earth metal pnictides with the cubic Th_3P_4 type: Synthesis and structure of $A_7Ga_2Sb_6$ (*A* = Sr, Ba, Eu). *J. Solid State Chem.* **2008**, *181*, 1909–1914. [CrossRef]
12. He, H.; Tyson, C.; Saito, M.; Bobev, S. Synthesis and structural characterization of the ternary Zintl phases $AE_3Al_2Pn_4$ and $AE_3Ga_2Pn_4$ (*AE* = Ca, Sr, Ba, Eu; *Pn* = P, As). *J. Solid State Chem.* **2012**, *188*, 59–65. [CrossRef]
13. Schäfer, M.C.; Suen, N.-T.; Bobev, S. Synthesis and crystal chemistry of new ternary pnictides containing lithium—Adding structural complexity one step at a time. *Dalton Trans.* **2014**, *43*, 16889–16901. [CrossRef] [PubMed]
14. You, T.-S.; Bobev, S. Cis-trans Germanium chains in the intermetallic compounds $ALi_{1-x}In_xGe_2$ and $A_2(Li_{1-x}In_x)_2Ge_3$ (*A* = Sr, Ba, Eu)—Experimental and theoretical studies. *J. Solid State Chem.* **2010**, *183*, 2895–2902. [CrossRef]

15. Suen, N.-T.; Guo, S.-P.; Hoos, J.; Bobev, S. Intricate Li–Sn disorder in rare-earth metal–lithium stannides. Crystal chemistry of $RE_3Li_{4-x}Sn_{4+x}$ (*RE* = La–Nd, Sm; x <0.3) and $Eu_7Li_{8-x}Sn_{10+x}$. *Inorg. Chem.* **2018**, *57*, 5632–5641. [PubMed]
16. Todorov, I.; Sevov, S.C. Heavy-metal aromatic and conjugated species: Rings, oligomers, and chains of tin in $Li_{9-x}EuSn_{6+x}$, $Li_{9-x}CaSn_{6+x}$, $Li_5Ca_7Sn_{11}$, $Li_6Eu_5Sn_9$, $LiMgEu_2Sn_3$, and $LiMgSr_2Sn_3$. *Inorg. Chem.* **2005**, *44*, 5361–5369. [CrossRef] [PubMed]
17. Todorov, I.; Sevov, S.C. Synthesis and characterization of $Na_2Ba_4Ga_2Sb_6$ and $Li_{13}Ba_8GaSb_{12}$. *Z. Kristallogr.* **2006**, *221*, 319–333. [CrossRef]
18. Suen, N.-T.; Bobev, S. Several new phases in *RE*–Mg–Ge systems (*RE* = rare-earth metal)—Syntheses, structures, and chemical bonding. *Eur. J. Inorg. Chem.* **2012**, 4141–4148. [CrossRef]
19. Monconduit, L.; Belin, C. A new ternary antimonide phase, LiBaSb. *Acta Crystallogr.* **2001**, *E57*, i17–i18. [CrossRef]
20. Gupta, S.; Ganguli, A.K. Synthesis, structure and properties of a new Zintl phase: SrLiSb. *J. Solid State Chem.* **2006**, *179*, 1318–1322. [CrossRef]
21. Liebrich, O.; Schäfer, H.; Weiss, A. Darstellung und Kristallstruktur von $Sr_3Li_4Sb_4$ und $Ba_3Li_4Sb_4$. *Z. Naturforsch. B* **1966**, *25b*, 650–651. [CrossRef]
22. Eisenmann, B.; Liebrich, O.; Schäfer, H.; Weiss, A. Darstellung und Kristallstruktur von CaLiSb. *Z. Naturforsch. B* **1969**, *24*, 1344–1345. [CrossRef]
23. Eisenmann, B.; Schäfer, H.; Turban, K. Neue intermetallische Verbindungen im anti-$PbCl_2$Typ. *Z. Naturforsch. B* **1975**, *30*, 677–680. [CrossRef]
24. Pauling, L. *The Nature of the Chemical Bond*; Cornell University Press: Ithaca, NY, USA, 1960.
25. Barrett, C.S.; Cucka, P.; Haefner, K. The crystal structure of antimony at 4.2, 78 and 298 K. *Acta Crystallogr.* **1963**, *16*, 451–453. [CrossRef]
26. Cucka, P.; Barrett, C.S. The crystal structure of Bi and of solid solutions of Pb, Sn, Sb and Te in Bi. *Acta Crystallogr.* **1962**, *15*, 865–872. [CrossRef]
27. Hönle, W.; von Schnering, H. Zur Struktur von LiP und KSb. *Z. Kristallogr.* **1981**, *155*, 307–314. [CrossRef]
28. Xia, S.-Q.; Bobev, S. Zintl phase variations through cation selection. Synthesis and structure of $A_{21}Cd_4Pn_{18}$ (*A* = Eu, Sr, Ba; *Pn* = Sb, Bi). *Inorg. Chem.* **2008**, *47*, 1919–1921. [CrossRef] [PubMed]
29. Emmerling, F.; Längin, N.; Petri, D.; Kroeker, M.; Röhr, C. Alkalimetallbismutide *A*Bi und ABi_2 (*A* = K, Rb, Cs)—Synthesen, Kristallstrukturen, Eigenschaften. *Z. Anorg. Allg. Chem.* **2004**, *630*, 171–178. [CrossRef]
30. Shannon, R.D. Effective ionic radii in oxides and fluorides. *Acta Crystallogr.* **1969**, *B25*, 925–946. [CrossRef]
31. Prakash, J.; Schäfer, M.C.; Bobev, S. Synthesis and structure determination of seven ternary bismuthides. Crystal chemistry of the $RELi_3Bi_2$ family (*RE* = La–Nd, Sm, Gd, Tb). *Acta Crystallogr.* **2015**, *C71*, 894–899.
32. Saparov, B.; He, H.; Zhang, X.; Greene, R.; Bobev, S. Synthesis, crystallographic and theoretical studies of the new Zintl phases $Ba_2Cd_2Pn_3$ (*Pn* = As, Sb), and the solid solutions $(Ba_{1-x}Sr_x)_2Cd_2Sb_3$ and $Ba_2Cd_2(Sb_{1-x}As_x)_3$. *Dalton Trans.* **2010**, *39*, 1063–1070. [CrossRef] [PubMed]
33. Guloy, A.M. *Inorganic Chemistry in Focus III*; John Wiley & Sons: Hoboken, NJ, USA, 2006.
34. Rehr, A.; Kuromoto, T.Y.; Kauzlarich, S.M.; Del Castillo, J.; Webb, D.J. Structure and properties of the transition-metal Zintl compounds $A_{14}MnPn_{11}$ (*A* = Ca, Sr, Ba; *Pn* = As, Sb). *Chem. Mater.* **1994**, *6*, 93–99. [CrossRef]
35. Brechtel, E.; Cordier, G.; Schäfer, H. Darstellung und Kristallstruktur von $Ca_9Mn_4Bi_9$ und $Ca_9Zn_4Bi_9$. *Z. Naturforsch. B* **1979**, *34*, 1229–1233. [CrossRef]
36. Ovchinnikov, A.; Prakash, J.; Bobev, S. Crystal chemistry and magnetic properties of the solid solutions $Ca_{14-x}RE_xMnBi_{11}$ (*RE* = La–Nd, Sm, and Gd–Ho; $x \approx 0.6$–0.8). *Dalton Trans.* **2017**, *46*, 16041–16049. [CrossRef] [PubMed]
37. Prakash, J.; Stoyko, S.; Voss, L.; Bobev, S. On the extended series of quaternary Zintl phases $Ca_{13}REMnSb_{11}$ (*RE* = La–Nd, Sm, Gd–Dy). *Eur. J. Inorg. Chem.* **2016**, 2912–2922. [CrossRef]
38. Xia, S.-Q.; Bobev, S. Interplay between size and electronic effects in determining the homogeneity range of the $A_9Zn_{4+x}Pn_9$ and $A_9Cd_{4+x}Pn_9$ Phases ($0 \leq x \leq 0.5$), *A* = Ca, Sr, Yb, Eu; *Pn* = Sb, Bi. *J. Am. Chem. Soc.* **2007**, *129*, 10011–10018. [CrossRef] [PubMed]
39. Wang, Y.; Bobev, S. Rare-earth Metal Substitutions in $Ca_{9-x}RE_xMn_4Sb_9$ (*RE* = La–Nd, Sm; $x \approx 1$). Synthesis and characterization of a new series of narrow-gap semiconductors. *Chem. Mater.* **2018**, *30*, 3518–3527. [CrossRef]

40. Xia, S.-Q.; Bobev, S. On the existence of Ca_2Bi—Crystal and electronic structure of Ca_4Bi_2O. *J. Alloys Compd.* **2007**, *427*, 67–72. [CrossRef]
41. Saparov, B.; Bobev, S. Synthesis, crystal and electronic structures of the new quaternary phases $A_5Cd_2Sb_5F$ (A = Sr, Ba, Eu), and $Ba_5Cd_2Sb_5O_x$ ($0.5 < x < 0.7$). *Dalton Trans.* **2010**, *39*, 11335–11343. [PubMed]
42. Ovchinnikov, A.; Saparov, B.; Xia, S.-Q.; Bobev, S. The ternary alkaline-earth metal manganese bismuthides Sr_2MnBi_2 and $Ba_2Mn_{1-x}Bi_2$ ($x \approx 0.15$). *Inorg. Chem.* **2017**, *56*, 12369–12378. [CrossRef] [PubMed]
43. Bruker. *SAINT*; Version 8.34a; Bruker Analytical X-ray Systems Inc.: Madison, WI, USA, 2013.
44. Sheldrick, G.M. *SADABS*; Version 2.10; Bruker Analytical X-ray Systems Inc.: Madison, WI, USA, 2001.
45. Sheldrick, G.M. Crystal structure refinement with *SHELXL*. *Acta Crystallogr.* **2015**, *C71*, 3–8.
46. Sheldrick, G.M. *SHELXT*-Integrated space-group and crystal-structure determination. *Acta Crystallogr.* **2015**, *A71*, 3–8. [CrossRef] [PubMed]
47. Gelato, L.M.; Parthé, E. *STRUCTURE TIDY*—A computer program to standardize crystal structure data. *J. Appl. Crystallogr.* **1987**, *20*, 139–143. [CrossRef]
48. Li, B.; Corbett, J.D. Phase stabilization through electronic tuning: Electron-poorer alkali-metal-indium compounds with unprecedented In/Li clusters. *J. Am. Chem. Soc.* **2005**, *127*, 926–932. [CrossRef] [PubMed]
49. Jepsen, O.; Burkhart, A.; Andersen, O.K. *The TB-LMTO-ASA Program, Version 4.7*; Max-Planck-Institut für Festkörperforschung: Stuttgart, Germany, 1999.
50. Von Barth, U.; Hedin, L. A local exchange-correlation potential for the spin polarized case: I. *J. Phys. C Solid State Phys.* **1972**, *5*, 1629–1642. [CrossRef]